Appl. Phys. B (2016) 122:63
DOI 10.1007/s00340-016-6333-z

Applied Physics B
Lasers and Optics

Effect of magnetic field on laser-induced breakdown spectroscopy of graphite plasma

Atiqa Arshad[1] · Shazia Bashir[1] · Asma Hayat[1] · Mahreen Akram[1] · Ayesha Khalid[1] · Nazish Yaseen[1] · Qazi Salman Ahmad[1]

Received: 19 October 2015 / Accepted: 11 January 2016 / Published online: 12 March 2016

Abstract The effect of transverse magnetic field on laser-induced breakdown spectroscopy of graphite plasma as a function of fluence has been investigated. Graphite targets were exposed to Nd:YAG (1064 nm, 10 ns) laser pulses at various laser fluences ranging from 0.4 to 2.9 J cm^{-2} under two different environment of air and Ar at a pressure of 150 and 760 torr. A transverse magnetic field of strength 0.5 tesla was employed by using permanent magnets. It is revealed that due to the presence of the magnetic field the emission intensity, electron temperature and number density of graphite plasma have been increased at all fluences and for all environmental conditions. The enhancement in plasma parameters is attributed to magnetic confinement effect and Joule heating effect. Initially by increasing the fluence from 0.4 to 1.5 J cm^{-2} (in air) and 0.4 to 1.8 J cm^{-2} (in Ar), the emission intensity, electron temperature and number density have been increased and have attained their maximum values. Further increase in fluence was responsible for the decreasing trend in all plasma parameters. More increase in fluence (beyond 1.8 J cm^{-2} in case of air and 2.2 J cm^{-2} in case of Ar) up to a maximum value of 2.9 J cm^{-2}, the saturation or self-sustained regime was achieved, which is responsible for insignificant changes in plasma parameters. The value of plasma parameter "β" was also evaluated analytically, and it was less than one for all conditions (fluences as well as environments), which confirmed the existence of confinement effect.

✉ Shazia Bashir
shaziabashir@gcu.edu.pk

[1] Centre for Advanced Studies in Physics (CASP), Government College University (GCU), Lahore, Pakistan

1 Introduction

Laser-induced breakdown spectroscopy (LIBS) is recognized as a powerful tool for elemental analysis of solids, liquids, gases and aerosol samples [1–4]. It is simple, fast, real time, in situ technique without the requirements of sample preparation [5]. It is also a valuable technique for the evaluation of electron temperature and number density of laser-induced plasma [6].

In recent years, the use of magnetic field to confine the laser-produced plasma has become significantly important [7, 8]. Magnetic field can be used to control the dynamical properties of transient and energetic plasmas in efficient ways. The plasma magnetic field interaction is used to study inertial fusion confinement, solar wind evolution, astrophysical jets, propagation of charged particle beams and bipolar flows associated with young stellar objects [9, 10]. Laser-based methods are used for measuring the deposition of material and retention of plasma fuel on the walls of fusion devices, without the removal of plasma-facing components [11]. LIBS is also used for diagnostics of fuel retention as well as removal and composition in international thermonuclear experimental reactors for future fusion devices [12]. The magnetic field is used for divergence and controlling the ion debris in extreme ultraviolet (EUV) lithography laser-produced plasma (LPP) sources [13, 14]. Droplet-free thin films can also be fabricated by use of magnetic field in pulsed laser deposition [15]. The expansion of laser-induced plasma in the presence of magnetic field may initiate several physical phenomena including plume confinement [16], Joule heating effect [17], conversion of plasma thermal energy into kinetic energy, plasma instabilities, emission enhancement and ion acceleration [17].

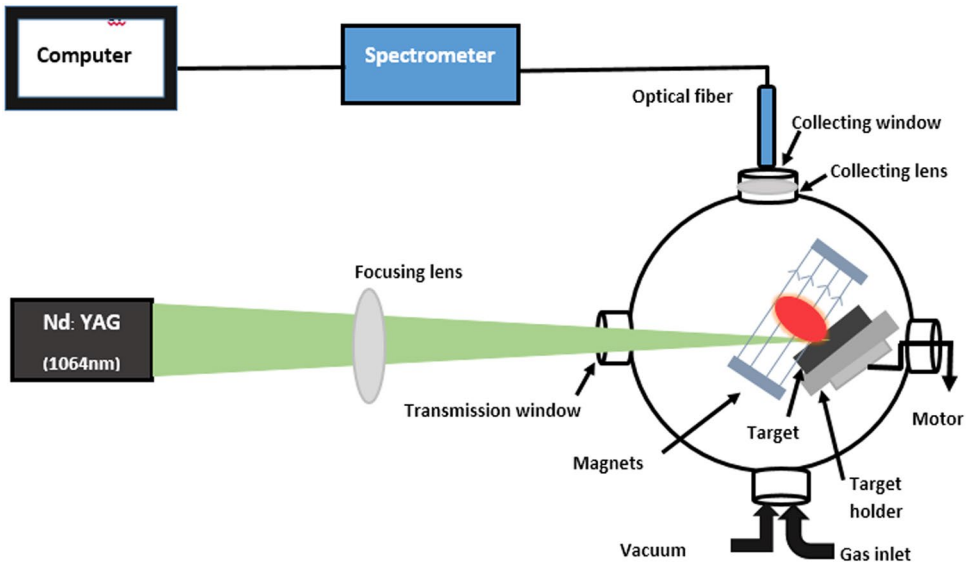

Fig. 1 Schematic of experimental setup for investigation of magnetic field effect on laser-induced breakdown spectroscopy of graphite plasma

Many groups have studied the interaction of expanding plasma with magnetic field. Bhadra [18] reported that a laser-produced plasma explosion is stopped by a magnetic field B at a distance of $R \sim B^{-2/3}$. Neogi and Thareja [19, 20] investigated laser-induced carbon plasma in a non-uniform magnetic field by using fast photography and emission spectroscopy. They observed oscillations in the temporal evolution of emission species, which were attributed to edge instability. Effect of strong external magnetic field (~20 T) on laser-produced plasma is reported by Pisarczyka et al. [21]. They reported that uniform and elongated plasma column was formed on the axis of magnetic coils. They also investigated X-rays and population inversion in the magnetically confined plasma. Kokai et al. [16] reported that during the laser ablation of graphite plasma, the growth of carbon clusters is enhanced in the presence of the magnetic field. They explained it as the ion neutral reaction due to an increase in ionic species, resulting from the collisional ionization of neutral species through confinement of electrons, which leads to growth of large carbon clusters. Rai et al. [22] studied the optical properties from liquid and solid samples and revealed that when these plasmas interact with steady magnetic field of about 0.5 T, an enhancement of emission was observed about 1.5–2 times. Joshi et al. [23] observed the effect of transverse magnetic field on plasma plume emissions of laser-produced Li plasma by atomic analysis. Harilal et al. [17] investigated the effect of transverse magnetic field on laser-produced aluminum plasma. They observed the change in plume structure and dynamics, an enhancement in emission, ionization and velocity due to the presence of the magnetic field by using fast photography, emission spectroscopy and time-of-flight spectroscopy. The effect of axial magnetic field on dynamics of laser-induced tin plasma was investigated by Roy et al. [7]. They investigated that both the electron temperature and electron density were increased by employing magnetic field at various distances from the target. Li et al. [5] studied the effect of magnetic field (0.8 T) on laser-induced copper plasma by employing spectral- and temporal-resolved emission spectroscopy. An enhancement of all spectral lines for all neutral, singly and doubly ionized species is observed. They also observed the effect of magnetic field on plasma parameters.

The enhancement in the emission intensity, electron temperature and number density is expected due to confinement as well as adiabatic compression and Joule heating effect. In order to confirm that magnetic field effect is responsible for enhancement of plasma parameters, experiment was performed at eight various fluences ranging from 0.4 to 2.9 J cm^{-2}. Nd:YAG laser (1064 nm, 10 ns, 10 Hz) was used as a source of irradiation. Graphite plasma is generated similarly at two different environments of air and Ar. These two gases are filled at two different pressures of 150 and 760 torr independently. The spectral lines of graphite plasma are measured by LIBS spectrometer. The electron temperature and number density of plasma are evaluated by using Boltzmann distribution and Stark broadening.

The confinement effects of magnetic field on graphite plasma can make it more useful in thin-film deposition of diamond-like carbon (DLC), ion implantation, nanostructuring of carbon, carbon nanotubes, nanowires, graphene, etc.

2 Experimental setup

The schematic setup of experimental setup for detection and analysis of spectral lines of laser-induced graphite plasma

along with employment of magnetic field is shown in Fig. 1. A Q-switched Nd:YAG laser 1064 nm (CRF 200: Big Sky laser Technologies, Quantral, France) with pulse duration of 10 ns, with a pulse energy ranging from 25 to 200 mJ and at repetition rate of 10 Hz was employed for plasma generation. Rectangular-shaped graphite (C) material with dimension $20 \times 20 \times 10\text{mm}^3$ was used as a target material. Before laser treatment, samples were grinded and then cleaned with acetone for the removal of contamination. Graphite targets, after mounting on sample holder, were placed in stainless steel chamber. The chamber was evacuated to the residual base pressure 10^{-3} mbar by using rotary pump. Two permanent magnets of diameter 2.8 cm with magnetic field strength 0.5 T which measured by Tesla coil were used to generate transverse magnetic field. The magnets were fixed in Teflon casing and were placed parallel to each other at a distance of 7 cm. They were mounted on aluminum holder at a height of 6.3 cm from the bottom of the chamber. Graphite target was placed in such way that it was at equal distance from both magnets as shown in Fig. 1. The laser beam generates the plasma after passing through a focusing lens of a focal length 50 cm by hitting target at an angle of 45° normal to the surface. The diameter of focused spot size was 116 μm. The magnets were placed in such way that magnetic field lines were perpendicular to the plasma plume expansion. For minimum relevant breakdown of environmental gases, the graphite targets were exposed at a distance 49.7 cm from the focusing lens (which is less than focal length).

The spectra were analyzed by LIBS spectrometer system (LIBS 2500 plus) with spectral range of 200–980 nm at a resolution of ±0.1 nm and integration time of 2.1 ms. The delay time of 1.25 μs between the laser trigger and data collection was kept constant for all measurements. The emission spectra were collected by collecting lens of focal length 5 cm and were transmitted by optical fiber to CCD arrays. The OLIBS software was used to analyze the data.

All measurements of laser-induced breakdown spectroscopy were taken in the presence and the absence of magnetic field.

The following four sets of experiments were performed:

1. Air was filled in vacuum chamber at a pressure of 150 torr. The first set of experiment was performed by exposing the graphite target to laser pulses at eight different energies ranging from 25 to 200 mJ corresponding to laser fluences of 0.4–2.9 J cm^{-2}.
2. Similarly, second set of experiment was performed by filling air at a pressure of 760 torr. LIBS analysis was performed at same parameters as have been employed for experiment 1.
3. In order to explore the effect of magnetic field on graphite plasma in the presence of environmental gases, the third set of experiment was performed by filling Ar gas at a pressure of 150 torr. The emission spectra were collected for same parameters as were used in experiments 1 and 2.
4. The fourth and last set of experiments was done by filling Ar gas at a pressure of 760 torr under similar conditions as have been used for experiments 1, 2 and 3.

3 Results and discussion

LIBS spectra of graphite plasma in the spectral range from 300 to 900 nm, obtained at a laser fluence of 1.5 J cm^{-2} in the presence of Ar at a pressure of 150 torr, are shown in Fig. 2 (a) without magnetic field and (b) with magnetic field.

3.1 Effect of magnetic field on graphite plasma parameters in air

3.1.1 Emission intensity

Graphs of Fig. 3 show the variation in the emission intensity of graphite plasma for the selected spectral lines of 473.51, 602.85 and 612.08 nm as function of laser fluence in air in the absence and presence of the magnetic field at

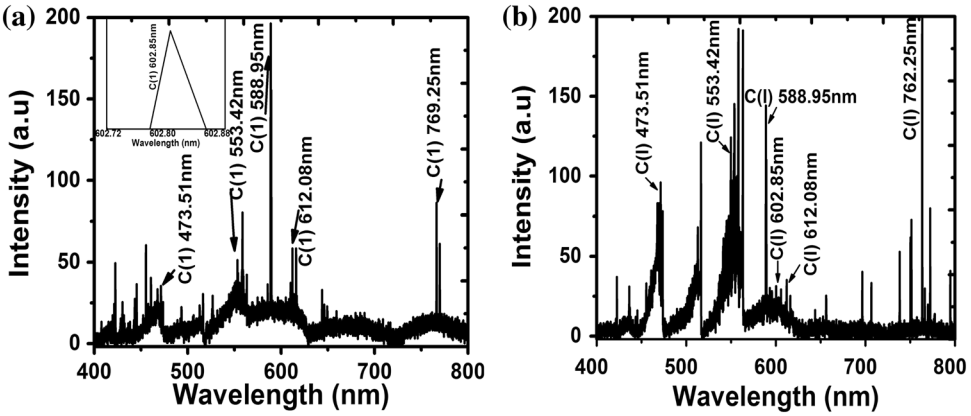

Fig. 2 Emission spectra of laser-induced graphite plasma collected in the presence of Ar at a pressure of 150 torr **a** without magnetic field **b** with magnetic field

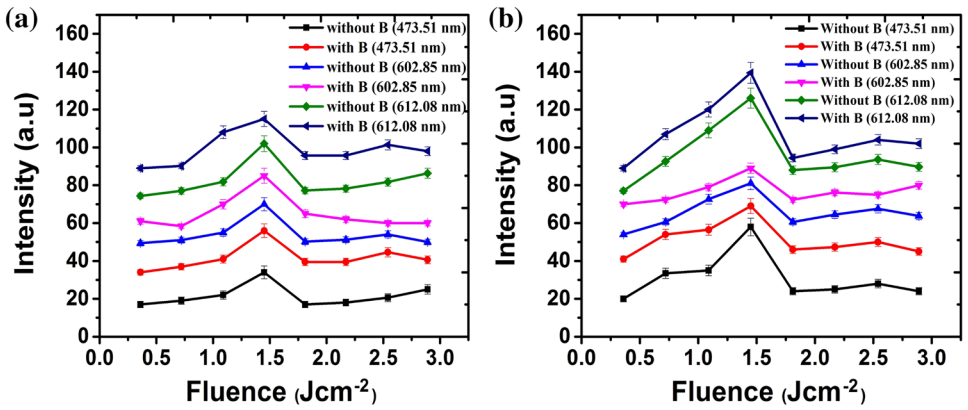

Fig. 3 Emission intensity of laser-produced graphite plasma at various fluences in air in the absence and presence of magnetic field at a pressure of **a** 150 torr and **b** 760 torr

Table 1 Relevant spectroscopic data of laser-produced graphite plasma taken from NIST database [25]

Wavelength (nm)	Transitions	Energy of upper level E_m (cm^{-1})	Statistical weight g_m	Transition probabilities (10^8 s^{-1})
473.51	$2s^2 2p5p \rightarrow {}^3P$	85203.6	5	0.000457
602.85	$2s^2 2p5d \rightarrow {}^3F^\circ$	86327.2	7	0.000481
612.08	$2s^2 2p7\ s \rightarrow {}^3P^\circ$	87718.5	5	0.002

a pressure of (a) 150 torr and (b) 760 torr. They depict that emission intensity increases with increasing laser fluence and achieves its maxima at fluence of 1.5 J cm^{-2}. With further increase in laser fluence from 1.5 to 1.8 J cm^{-2}, decreasing trend in emission intensity is observed. When fluence is increased from 1.8 J cm^{-2} to a maximum value of 2.9 J cm^{-2}, the intensity of emission lines shows insignificant changes and the possible mechanisms responsible for this behavior are explained in discussion section. The value of emission intensity is observed to be higher for all spectral lines in the presence of the magnetic field as compared to non-magnetized plasma. Similarly, it is also revealed that all spectral lines show their maxima at the same fluence of 1.5 J cm^{-2} for both pressures. The comparison of Fig. 3a, b shows that the emission intensity of graphite plasma in air is greater for high pressure of 760 torr as compared to lower pressure of 150 torr. It is true for all spectral lines observed without and with magnetic field. These results reveal that laser fluence, magnetic field and pressure of environmental gas play a key role for controlling the emission intensity of spectral lines.

3.1.2 Electron temperature

The electron temperature is responsible for various excitations and ionization processes that occur in laser-induced plasmas (LIPs). To calculate the electron temperature, plasma is assumed to be in local thermodynamical equilibrium (LTE), and the population of excited atoms follows the Boltzmann distribution, which is governed by following equation [24]:

$$\ln\left(\frac{\lambda_{mn} I_{mn}}{g_m A_{mn}}\right) = -\frac{E_m}{KT_e} + \ln\left(\frac{N(T)}{U(T)}\right) \quad (1)$$

where λ_{mn}, I_{mn}, A_{mn} are wavelength, intensity, transition probability of the upper and lower state.E_m and g_m are the energy of the upper state and statistical weight, and T_e, $U(T)$, $N(T)$ and K are electron temperature, partition function, total number density and Boltzmann constant, respectively. By assuming that distribution is the Boltzmann, a straight line is fitted by plotting of a logarithmic term on left-hand side versus E_m whose slope is equal to $-1/kT_e$. Electron temperature is evaluated by the selection of three transition lines of graphite plasma at 473.51 nm ($2s^2 2p5p^\circ \rightarrow {}^3P$), 602.85 nm ($2s^2 2p5d \rightarrow {}^3F^\circ$) and 612.08 nm ($2s^2 2p7\ s \rightarrow {}^3P^\circ$). The relevant spectroscopic data of graphite plasma used for valuation of electron temperature are taken from NIST database [25] and are listed in Table 1. Graphs of Fig. 4 reveal variations of electron temperature of graphite plasma in air as function laser fluence with and without magnetic field at a pressure of (a) 150 torr and (b) 760 torr. It is revealed from these figures that electron temperature increases with increasing laser fluence and achieves its maxima at a laser fluence of 1.5 J cm^{-2}. When laser fluence is increased from 1.5 to 1.8 J cm^{-2}, the electron temperature decreases significantly. With further increase in laser fluence from 1.8 J cm^{-2} to maximum value 2.9 J cm^{-2}, it is observed that electron temperature remains constant with insignificant changes. This region can be considered as saturation region of graphite plasma. Various physical processes responsible for three different trends of excitation temperatures are

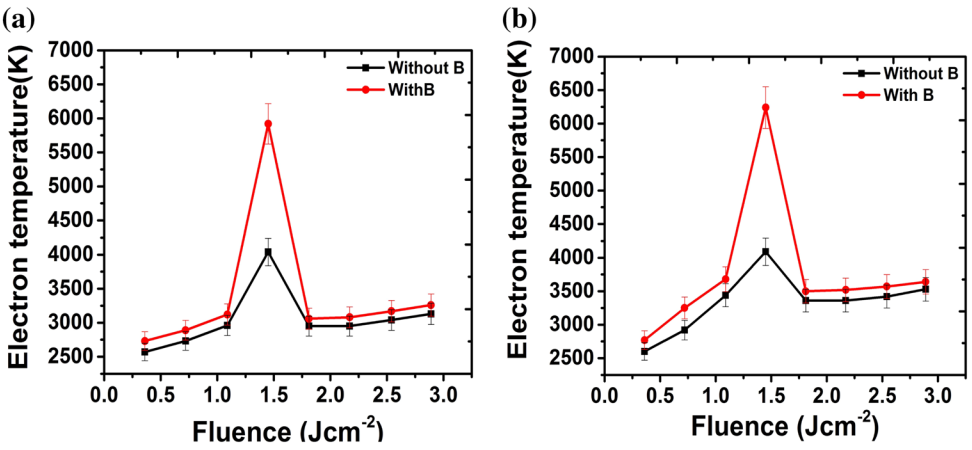

Fig. 4 Variation of electron temperature of graphite plasma as a function of laser fluence with and without magnetic field in air at pressure of **a** 150 torr and **b** 760 torr

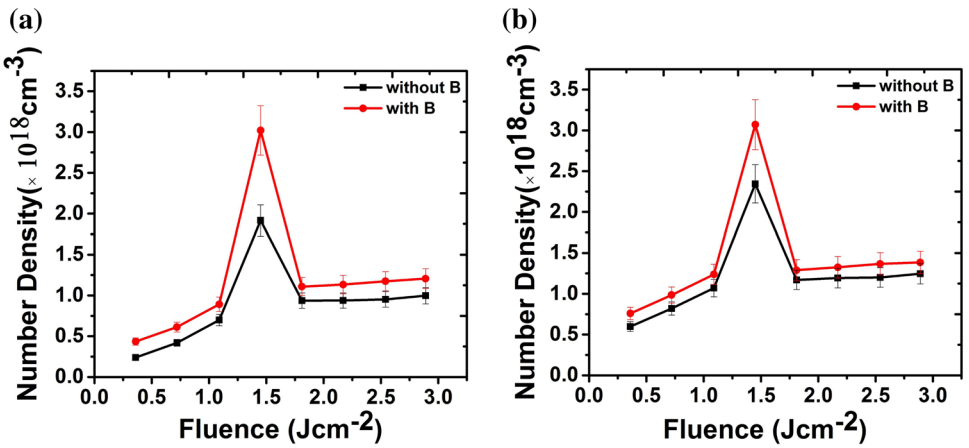

Fig. 5 Variation of number density of graphite plasma as a function of laser fluence with and without magnetic field in air at a pressure of **a** 150 torr and **b** 760 torr

explained in discussion section. From both Fig. 4a, b, it is observed that electron temperature is higher in the presence of magnetic field for both pressures. However, greater value of electron temperature is observed at high air pressure of 760 torr.

If collisional process dominates over radiative process, then plasma is considered to be in local thermal equilibrium (LTE). The McWhirter criteria for lower limit of number density are given by [26]:

$$n_e \geq 1.6 \times 10^{12} T^{1/2} \Delta E^3 \tag{2}$$

where T is the plasma temperature (K), and ΔE is the energy gap between the two states (eV). At $T = 7050$ K (the maximum calculated temperature), the calculated electron number density is $n_e \sim 4.3 \times 10^{12}$ cm^3, which fulfills the local thermal equilibrium condition (LTE).

3.1.3 Electron number density

The electron number density is estimated using stark broadening of an isolated graphite line. Plasma species are under the influence of electric field of fast-moving electrons and slow-moving ions. The perturbing electric field shifts the energy level of species, which is leading to broadening, regarding Stark broadening. Pressure and Doppler broadening contribute insignificantly and hence can be neglected. The electron number density can be related to full width at half maximum [FWHM ($\Delta\lambda_{1/2}$)] of Stark-broadened line by the relation [27]:

$$\Delta\lambda_{\frac{1}{2}} = 2w\left(\frac{n_e}{10^{16}}\right) + 3.5A\left(\frac{n_e}{10^{16}}\right)^{1/4}\left[1 - 1.2N_D^{-1/3}\right] \times w\left(\frac{n_e}{10^{16}}\right) \tag{3}$$

where A is ion broadening, and w is the electron impact width parameter. N_D(cm^{-3}) is number of the particles in the Debye sphere. The first term in Eq. 3 is due to electrons broadening, and the second term is due to ions broadening, which can be ignored due to minor contribution. Therefore, Eq. 3 reduces to the following expression:

$$\Delta\lambda_{1/2} = 2w\left(\frac{n_e}{10^{16}}\right) \tag{4}$$

The graphite line (I) at wavelength of 602.85 nm is used to calculate the electron number density under the consideration that line is not self-absorbed and its shape is well fitted by the Lorentzian function. Graphs of Fig. 5 show the

variation of electron number density of graphite plasma in air as a function of laser fluence without and with magnetic field at a pressure of (a) 150 torr and (b) 760 torr. It is observed from Fig. 5a, b that electron number density increases with increasing laser fluence and achieves its maxima at fluence of 1.5 J cm^{-2}. With further increase in laser fluence, the number density decreases significantly and shows the same trend as is observed for electron temperature. For higher fluence regime ranging from 1.8 J cm^{-2} to maximum value of 2.9 J cm^{-2}, the number density almost remains constant with insignificant changes. This fluence regime is responsible for saturation of plasma parameters. Graphs of Fig. 5a, b depict that number density of graphite plasma is enhanced due to the employment of magnetic field for both pressures (150 and 760 torr) of the air. However, the maximum value of number density is obtained at 760 torr.

3.2 Effect of magnetic field on graphite plasma parameters in Ar

3.2.1 Emission intensity

Graphs of Fig. 6 show the variations of emission intensity of graphite plasma as a function of laser fluence without and with magnetic field in the presence of Ar as an environmental gas at a pressure of (a) 150 torr and (b) 760 torr. In Ar environment, the maximum value of emission intensity is achieved at laser fluence of 1.8 J cm^{-2} for both pressures (150 and 760 torr). Again, it is revealed that the emission intensity is enhanced in the presence of the magnetic field in Ar environment. The maximum emission intensity is observed for high pressure of 760 torr in the presence of 0.5 T magnetic field. The comparison of Figs. 6a, b with 3a, b shows that emission intensity in case of Ar environment is higher as compared to air.

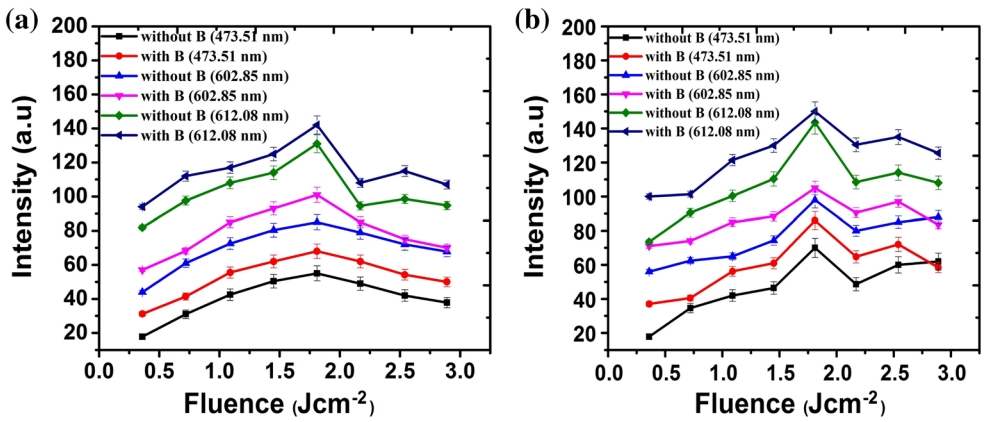

Fig. 6 Variation of emission intensity of graphite plasma as a function of laser fluence without and with magnetic field in the presence of Ar as an environmental gas at a pressure of **a** 150 torr and **b** 760 torr

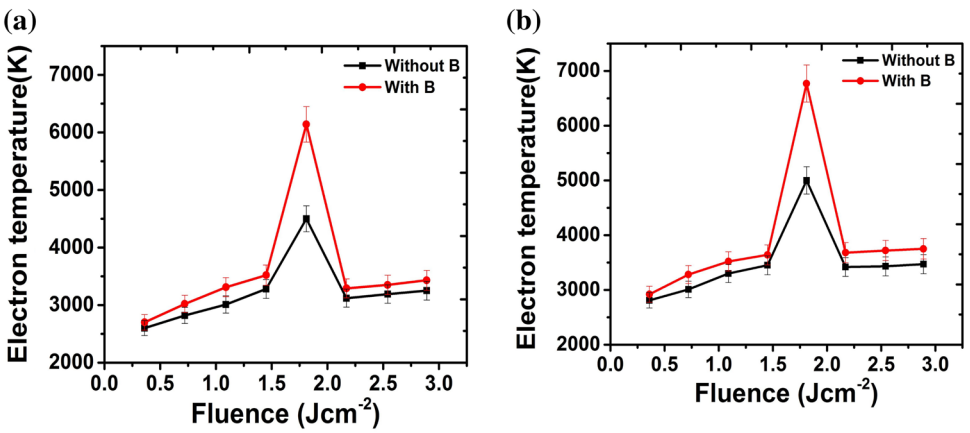

Fig. 7 Variation of electron temperature of graphite plasma in the presence and in the absence of magnetic field as a function of laser fluence under Ar environment at a pressure of **a** 150 torr and **b** 760 torr

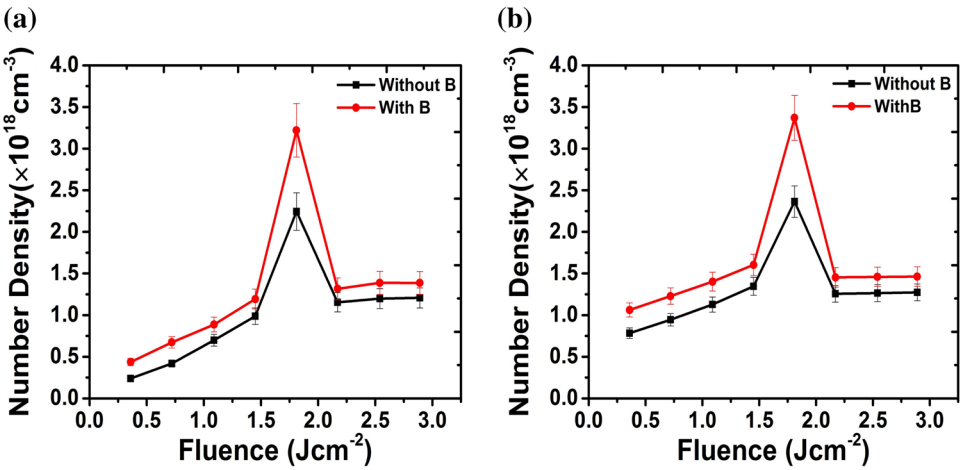

Fig. 8 Variation of number density of graphite plasma as a function of laser fluence under Ar ambient environment without and with magnetic field at two different pressures of **a** 150 torr and **b** 760 torr

Table 2 Evaluated values of plasma parameter β, maximum and minimum values of electron temperature and number density of graphite plasma, without and with magnetic field, in the presence of air and Ar, at two different pressures of 150 and 760 torr

	Without magnetic field				With magnetic field			
	Air 150 torr	Air 760 torr	Ar 150 torr	Ar 760 torr	Air 150 torr	Air 760 torr	Ar 150 torr	Ar 760 torr
T_e (K) (maximum)	4040	4090	4500	5000	5920	6240	6140	6770
T_e (K) (minimum)	2570	2600	2600	2810	2730	2770	2700	2920
n_e ($\times 10^{18}$ cm^{-3}) (maximum)	1.92	2.35	2.25	2.36	3.02	3.08	3.22	3.37
n_e ($\times 10^{18}$ cm^{-3}) (minimum)	0.24	0.59	0.23	0.78	0.44	0.75	0.44	1.06
β (for maximum value)	–	–	–	–	0.0021	0.0023	0.0024	0.0027
β (for minimum value)	–	–	–	–	0.0001	0.0002	0.0001	0.0004

3.2.2 Electron temperature

Graphs of Fig. 7 show the variations of electron temperature of graphite plasma in the presence and also in the absence of magnetic field as a function of laser fluence under Ar environment at a pressure of (a) 150 torr and (b) 760 torr. The maximum value of electron temperature is achieved at laser fluence of 1.8 J cm^{-2} for both pressures of Ar. It depicts that electron temperature enhances in the presence of magnetic field, and maximum value of electron temperature is observed at a pressure of 760 torr. The trend of electron temperature as a function of laser fluence in Ar (150 and 760 torr) remains similar to that observed in case of air (150 and 760 torr) with the only difference that maxima in case of Ar are achieved at laser fluence of 1.8 J cm^{-2}, in contrast to 1.5 J cm^{-2} in air.

3.2.3 Electron number density

Graphs of Fig. 8 reveal the variations of electron number density of graphite plasma in the presence and also in the absence of magnetic field as a function of laser fluence under Ar environment at a pressure of (a) 150 torr and (b) 760 torr. The trend of electron number density as a function of laser fluence in Ar (150 and 760 torr) remains similar to that observed in case of air (150 and 760 torr) with the only difference that maxima in case of Ar are achieved at laser fluence of 1.8 J cm^{-2}. The maximum electron number density is observed at 1.8 J cm^{-2} for both pressures (150 and 760 torr). It is observed that number density increases in the presence of magnetic field and that maximum value is obtained at a pressure of 760 torr in Ar. The trend of electron number density is similar to electron temperature for both environments.

4 Discussion

The results obtained from LIBS reveal that the emission intensity, electron temperature and number density are strongly affected by magnetic field, in different environments and their corresponding pressures. The values of the emission intensity, electron temperature and number density are higher for Ar than air. Similarly for a pressure of 760 torr, all plasma parameter values are greater than those of 150 torr for both environments, i.e., air and Ar. Maximum and minimum values of electron temperature and number density of graphite plasma, without and with

magnetic field, in the presence of air and Ar, at two different pressures of 150 torr and 760 torr, are listed in Table 2.

Initially, at low fluence the ablation rate increases with increasing laser fluence, which in turn increases the electron temperature and number density [28]. If plasma reaches its maximum value of temperature and number density, then plume absorbs laser energy continuously through inverse bremsstrahlung, and photo ionization processes and shields the target from incoming laser irradiation [29]. With the increasing laser fluence, the electron temperature and number density decrease because less energy is deposited on the target's surface due to shielding effect of plasma. There could be two possible reasons for the decrease in emission intensity of graphite spectral lines: first is the self-absorption of emission lines or second is the reflection of laser fluence by the magnetic field confined plasma in the presence of magnets after a fluence of 1.5 J cm^{-2} in case of air and 1.8 J cm^{-2} in case of Ar [22]. At higher laser fluence, the saturation region is observed due to the self-regulating regime in addition to the shielding effect [30].

In plasma, the rate of change of electron temperature is a combination of three terms: electron heating due to collisional de-excitation of metastable ions, elastic collision and recombination of ions [24]. When the pressure increases inside the plasma, inelastic collision increases due to greater confinement effects of plasma. At 760 torr pressure, the highest value of electron temperature is observed, because electrons gain energy through recombination of ions and collisional de-excitation [24]. The following relation explains the inelastic collision rate at which electrons lose their energy with respect to electron temperature [31].

$$Q_{\Delta t} = \frac{2m_e}{M_B}\sigma_{ea}\, n_B\, [5kT_e/\pi m_e]^{1/2} \tag{5}$$

where σ_{ea} illustrates the elastic scattering of the electron cross section. M_B is the mass and n_B represents the density of background gas atoms. M_B is inversely proportional to the cooling. Thus, lighter gases are effective for rapid cooling (air is rapid cooler than Ar).

As described in Figs. 3, 4, 5, 6, 7 and 8, the emission intensity, electron temperature and number density are higher in case of Ar than air. It is attributed to the fact that the cascade condition is more favorable in the case of Ar as compared to air. For the development of cascade-like growth, the necessary condition is given by the following relation [27].

$$\frac{d\varepsilon}{dt} = \frac{4\pi^2 e^2 I \nu_{eff}}{m_e c\omega^2} - \frac{2m_e \nu_{eff} E}{M} > 0 \tag{6}$$

where ε is the free electron energy, m_e is the mass of electron, e is charge of electron, M is mass of the neutral particle of the background gas, E is the first ionization energy of the gas, I is the irradiation intensity, ω is the cyclic frequency of the radiation and ν_{eff} is the effective electron-neutral collision. The first term of Eq. 6 remains same for all gases because it represents the growth rate of energy by the absorption of laser irradiation. Due to inelastic and elastic collisions with neutral particle of gas, the rate of energy loss of plasma is described by the second term of Eq. 6. In cascade growth, E/M is the decisive factor for energy loss calculation. The calculated values of E/M are 0.39, 0.52 and 0.43 for Ar, N_2 and O_2, respectively, which confirm that cascade condition is more favorable in the case of Ar than air.

When transverse magnetic field is applied, the emission intensity, electron temperature and number density of graphite plasma are increased as compared to the absence of magnetic field. It is attributable to the fact that transverse magnetic field significantly slows down the propagation of the ablated plume and consequently confinement effects occur [32]. The plume front penetrates into the magnetic field during the confinement, but it is not fully stopped by magnetic field. It is reported that along the axial direction, the peak expansion velocity is higher as compared to radial expansion velocity [32]. The interior of the plasma is shielded by the outer layer of the plasma from the magnetic field, which influences the magnetic field interaction and magnitude [32]. The Lorentz force influences ions and electrons in the plasma, when magnetic field is applied to the LIPs. Magnetic field decelerates expansion as well the as diffusion of plasma. The parameter β of plasma from magneto-hydro-dynamics (MHD) equations is given by [33]:

$$\beta = \frac{8\pi n_e kT_e}{B^2} = \frac{\text{Particle or thermal pressure}}{\text{Magnetic field pressure}} \tag{7}$$

where B is the magnetic field (G), n_e represents the electron number density (cm^{-3}), k illustrates the Boltzmann constant and electron temperature is the (eV). The ratio of particle pressure to magnetic field pressure is the plasma parameter β, and it indicates the size of diamagnetic effect. The deceleration of the plasma expansion under the effect of externally applied magnetic field is given as [34]:

$$\frac{v_2}{v_1} = \left(1 - \frac{1}{\beta}\right)^{1/2} \tag{8}$$

where v_1 is the asymptotic plasma expansion velocity in the absence and v_2 in the presence of magnetic field. The magnetic field stops the plasma, when $\beta = 1$. The magnetic confinement will be effective for $\beta < 1$. The magnetic confinement does not remain effective for $\beta > 1$. Using Eq. 7, the values of β are estimated for maximum as well as minimum value of electron temperature and number density for both

environments of air and Ar at a pressure of 150 and 760 torr and are listed in Table 2. The analytical value of β is smaller than 1 for all cases and hence provides the proof for the existence of plume magnetic confinements. Therefore, the magnetic plasma can be treated as a compressible fluid [35].

As can be seen from Figs. 3a, b and 6a, b, the emission intensities of all spectral lines are enhanced in the presence of magnetic field. The magnetic confinement of LPP is the main reason for effect of enhancement. As the plasma plume expands across the magnetic field, the electrons and ions will be separated by Lorentz force in the direction perpendicular to magnetic field and mass flow velocity [36]. This current generates a deep force in the direction of plasma plume expansion, which decelerates the bulk of plasma. Thus, due to the presence of the magnetic field, the expansion of the plasma decelerates. The emission intensities are significantly increased because the collision excitation and rate of recombination are increased, when the plasma is confined. It is reported previously [20] that for carbon, the magnetic field enhances the optical emissions from ionic and atomic species in the plume.

The two effects: adiabatic compression of plasma by magnetic field and resistive Ohmic/Joule heating effect also cause the increase in electron temperature, in the presence of external magnetic field [17]. The magneto hydrodynamic (MHD) model can be used to understand Joule heating effect, which describes the expansion of ionized plasma in magnetic field. In the plasma, the generalized form of Ohm's law is given by [37]:

$$E + V \times B = J/\sigma_0 + (J \times B)/n_e e \tag{9}$$

where E and B are the electric and magnetic field fields, V is the mass flow velocity, J is the electron conduction current, and σ_0 the conductivity, n_e is the density of charge particles and e is the electric charge. When the plume expands across a magnetic field, work is performed against the term $J \times B$ that decelerates the flow. The heating occurs when the electrons gain energy from the plume kinetic energy and the force $J \times B$ compresses the plasma until the kinetic pressure equals the magnetic pressure. That is why electrons continue to excite toward higher charge states and lead to Joule heating effect. Electron's collisional ionization increases by magnetic field, which increases the ion by both electron temperature and number density [35].

The electron number density increases in the presence of 0.5 T magnetic field in Ar and air for both pressures of 150 and 760 torr. The plasma is confined in a smaller region due to magnetic confinement and correspondingly the electron number density increases. The number density can be estimated from mass ablation rate mechanism (that is $dm/dt \propto I^{0.6}$). The number density increases in external magnetic field as compared to field free case because the velocity of bulk plasma decreases in the presence of magnetic field [38].

5 Conclusions

The influence of transverse magnetic field on graphite plasma parameters as a function of laser fluence has been investigated under ambient environments of air and Ar at two different pressures of 150 and 760 torr. It was found that all plasma parameters, i.e., emission intensity, electron temperature and number density, are increased in the presence of the transverse magnetic field. These results confirm that magnetic field is responsible for significantly enhancing the plasma parameters for all fluences and environmental conditions. The other influencing factors for plasma parameters are fluence as well as nature and pressure of environmental gases. It was observed that maximum values of emission intensity, electron temperature and number density are obtained at fluence of 1.5 J cm^{-2} in case of air environment for both pressures of 150 and 760 torr. In case of Ar environment, maximum value of emission intensity, electron temperature and number density are achieved at 1.8 J cm^{-2} at a pressure of 150 and 760 torr. However, higher pressure of 760 torr is responsible for enhanced emission intensity, electron temperature and number density as compared to lower pressure of 150 torr, and it is true for both environments. It is also observed both electron temperature and electron number density have greater values in case of Ar environment as compared to air. The effect of magnetic field on graphite plasma can make it more useful in various scientific and industrial applications, e.g., thin-film deposition of diamond-like carbon (DLC), carbon ion implantation using laser-induced graphite plasma as ion source, micro/nanostructuring of carbon, fabrication of carbon nanotubes, nanowires and graphene. In addition, the confined plasma in the presence of magnetic can be used in inertial confinement fusion by employing high-intensity lasers. In future, laser-induced breakdown spectroscopy of metallic, insulating and semiconducting materials in the presence of strong magnetic fields can be employed to increase the density and kinetic energies of ablated species. These generated species can become useful tool for surface, structural and mechanical modifications of the materials and will have tremendous applications in material science, medicine and industry. The employment of magnetic field on laser-induced plasma can be used as an analyzer for energy and mass separation of ions and isotopes according to their charge to mass ratio.

References

1. V. Sturm, L. Peter, R. Noll, Steel analysis with laser induced breakdown spectroscopy in the vacuum ultraviolet. Appl. Spectrosc. **54**, 1275–1278 (2000)

2. A.P.M. Michel, M. Lawrence-Snyder, S.M. Angel, A.D. Chave, Laser induced breakdown spectroscopy of bulk aqueous solution at oceanic pressures evaluation of key measurement parameters. Appl. Optics **46**, 2507–2515 (2007)
3. M. Hanafi, M.M. Omar, Y.D. Gamal, Study of laser induced breakdown spectroscopy of gases. Rad. Phys. Chem. **57**, 11–20 (2000)
4. D.W. Hahn, M.M. Lunden, Detection and analysis of aerosol particles by laser induced breakdown spectroscopy. Aerosol Sci. Technol. **33**, 30–48 (2000)
5. Y. Li, C. Hu, H. Zhang, Z. Jiang, Z. Li, Optical emission enhancement of laser-produced copper plasma under a steady magnetic field. Appl. Optics **48**, 105–110 (2009)
6. N.M. Shaikh, S. Hafeez, M.A. Baig, Comparison of zinc and cadmium plasma parameters produced by laser ablation. Spectrochim. Acta B **62**, 1311–1320 (2007)
7. A. Roy, S.S. Harilal, S.M. Hassan, A. Endo, Collimation of laser produced plasmas using axial magnetic field. Laser Part. Beams **33**, 1–8 (2015)
8. A. Kumar, S. George, R.K. Singh, H. Joshi, V.P.N. Nampoori, Image analysis of expanding laser produced lithium plasma plume in variable transverse magnetic field. Laser Part. Beams **29**, 241–247 (2011)
9. H.C. Pant, Laboratory simulation of space and astrophysical plasmas using intense lasers. Phys. Scr. **50**, 109–113 (1994)
10. M.V.Z.W. Gekelman, S. Vincena, P. Pribyl, Laboratory experiments on Alfve´n waves caused by rapidly expanding plasmas and their relationship to space phenomena. J. Geophys. Res. Space Phys. **108**, 1281–1291 (2003)
11. P. Gasior, M. Bieda, M. Kubkowska, R. Neu, J. Wolowski, ASDEX upgrade team, laser induced breakdown spectroscopy as diagnostics for fuel retention and removal and wall composition reactors with mixed material components. Fusion Eng. Des. **86**, 1239–1242 (2011)
12. V. Philipps, A. Malaquias, A. Hakola, J. Karhunen, G. Maddaluno, S. Almaviva, L. Caneve, F. Colao, E. Fortuna, P. Gaior, M. Kubkowska, A. Czarnecka, M. Laan, A. Lissovski, P. Paris, H.J. Van der Meiden, P. Petersson, M. Rubel, A. Huber, M. Zlobinski, B. Schweer, N. Gierse, Q. Xiao, G. Sergienko, Development of laser-based techniques for in situ characterization of the first wall in ITER and future fusion devices. Nucl. Fusion **53**, 093002–093012 (2013)
13. S.S. Harilal, M.S. Tillack, Y. Tao, B. O'Shay, R. Paguio, A. Nikroo, Extreme ultraviolet spectral purity and magnetic ion debris mitigation by use of low density tin targets. Opt. Lett. **31**, 1549–1551 (2006)
14. A. Roy, S.M. Hassan, S.S. Harilal, A. Endo, T. Mocek, A. Hassanien, Extreme ultraviolet emission and confinement of tin plasmas in the presence of magnetic field. Phys. Plasmas **21**, 053106–053111 (2014)
15. Y.Y. Tsui, H. Minami, D. Vick, R. Fedosejevs, Debris reduction for copper and diamond like carbon thin film produced by magnetically guided pulsed laser deposition. J. Vac. Sci. Technol. A **20**, 744–747 (2002)
16. F. Kokai, Y. Koga, R.B. Heimamann, Magnetic field enhanced growth of carbon cluster ions in the laser ablation plume of graphite. Appl. Surf. Sci. **96–98**, 261–266 (1996)
17. S.S. Harilal, M.S. Tillack, B. O'Shay, C.V. Bindhu, F. Najmabadi, Confinement and dynamics of laser-produced plasma expanding across a transverse magnetic field. Phys. Rev. E **69**, (026413-1)-(026413-11) (2004)
18. D.K. Bhadra, Expansion of resistive plasmoid in magnetic field. Phys. Fluids **11**, 234–239 (1968)
19. A. Neogi, R.K. Thareja, Laser-produced carbon plasma expanding in vacuum, low pressure ambient gas and nonuniform magnetic field. Phys. Plasma **6**, 365–371 (1999)
20. A. Neogi, V. Narayanan, R.K. Thareja, Optical emission studies of laser ablated carbon plasma in a curved magnetic field. Phys. Lett. **258**, 135–140 (1999)
21. T. Pisarczyka, A. Faryńskia, H. Fiedorowicza, P. Gogolewskia, M. Kuśnierza, J. Makowskia, R. Miklaszewskia, M. Mroczkowskia, P. Parysa, M. Szczureka, Formation of an elongated plasma column by a magnetic confinement of a laser-produced plasma. Laser Part. Beams **10**, 767–777 (1992)
22. V.N. Rai, A.K. Rai, F.Y. Yueh, J.P. Singh, Optical emission spectroscopy from laser induced breakdown plasma of solids and liquid samples in the presence of magnetic field. Appl. Optics **42**, 2085–2093 (2003)
23. A.K.H.C. Joshi, R.K. Singh, V. Prahlad, Effect of transverse magnetic field on the plume emission on the laser produced plasma: an atomic analysis. Spectrochim. Acta B **65**, 415–419 (2010)
24. S.S. Harilal, C.V. Bindhu, V.P.N. Nampoori, C.P.G. Vallabhan, Influence of ambient gas on the temperature and density of laser produced carbon plasma. Appl. Phys. Lett. **72**, 167–169 (1998)
25. NIST, National Institute of Standard and Technology. http://physics.nist.gov/cgi-bin/ASD/lines1.pl
26. A. Nakimana, H. Tao, X. Gao, Z. Hao, J. Lin, Effects of ambient conditions on femtosecond laser-induced breakdown spectroscopy of Al. J. Phys. D Appl. Phys. **46**, 285204–285210 (2013)
27. N. Farid, S. Bashir, K. Mehmood, Effect of ambient gas conditions on laser induced Cu plasma and surface morphology. Phys. Scri. **85**, 015702–015709 (2012)
28. W.F. Luo, X.X. Zhao, Q.B. Sun, C.X. Gao, J. Tang, H.J. Wang, W. Zhao, Characteristics of the aluminium alloy plasma by a 1064 nm Nd:YAG laser with different irradiance. Pramana J. Phys. **74**, 945–959 (2010)
29. S.S. Harilal, C.V. Bindhu, V.P.N. Nampoori, C.P.G. Vallabhan, Temporal and spatial behavior of electron density and temperature in a laser produced plasma from YBa_2 Cu_3 O_7. Appl. Spect. **52**, 449–455 (1998)
30. G. Cristofoetti, S. Legnaioli, V. Palleschi, E. Tognoni. P. A. Benedetti, Observation of different mass removal regimes during the laser ablation of an aluminium target in air. J. Anal. At. Spectrom. **23**, 1518–1528 (2008)
31. S. Bashir, N. Farid, K. Mahmood, M.S. Rafique, Influence of ambient gas and its pressure on the laser induced breakdown spectroscopy and the surface morphology of laser ablated Cd. Appl. Phys. A **107**, 203–212 (2012)
32. D.W. Koopman, High beta effects and anomalous diffusion in plasma expanding into magnetic field. Phys. Fluids **19**, 670–674 (1976)
33. F.F. Chen, *Introduction to plasma physics* (Plenum, New York, 1974)
34. V.N. Rai, M. Shukla, H.C. Pant, An X-ray biplanar photodiode and the X-ray emission from magnetically confined laser produced plasma. Pramana J. Phys. **52**, 49–65 (1999)
35. H. Lan, X.B. Wang, H. Chen, D.L. Zuo, P.X. Lu, Influence of a magnetic field on laser-produced Sn plasma. Plasma Sources Sci. Technol. **24**, 055012–055019 (2015)
36. J.A. Bittencourt, *Fundamentals of plasma physics* (Pergamon, Oxford, 1986)
37. T.J.M. Boyd, J.J. Sanderson, *The physics of plasmas* (Cambridge University Press, New York, 2003)
38. A. Neogi, R.K. Thareja, Dynamics of laser produced carbon plasma expanding in a nonuniform magnetic field. J. Appl. Phys. **85**, 1131–1136 (1999)